Chinese Chemical Letters 37 (2026) 111507

Contents lists available at ScienceDirect

Chinese Chemical Letters

journal homepage: www.elsevier.com/locate/cclet

Pressure-induced tunable photoluminescence of Mn-doped post-perovskites (TDMP)$PbBr_4$

Ruijing Fu[a,d], Junpeng Gao[a], Lingrui Wang[b], Bin Xiao[a], Guangxia Wang[a,*], Qingguang Zeng[a,d,*], Guanjun Xiao[c,*]

[a] School of Applied Physics and Materials, Wuyi University, Jiangmen 529020, China
[b] Key Laboratory of Materials Physics, Ministry of Education, School of Physics, Zhengzhou University, Zhengzhou 450052, China
[c] State Key Laboratory of High Pressure and Superhard Materials, College of Physics, Jilin University, Changchun 130012, China
[d] Institute of Carbon Peaking and Carbon Neutralization, Wuyi University, Jiangmen 529020, China

ARTICLE INFO

Article history:
Received 23 April 2025
Revised 20 June 2025
Accepted 25 June 2025
Available online 25 June 2025

Keywords:
High pressure
Piezochromism
Mn-doped perovskite
Emission color modulation
One-dimensional organic-inorganic halide perovskite

ABSTRACT

One-dimensional (1D) organic-inorganic halide perovskites have produced significant research interest due to their unique structure and superior tunable luminescence properties. Here, we successfully achieved a unique color-tunable phenomenon of Mn-doped 1D post-perovskite (TDMP)$PbBr_4$ (TDMP = *trans*-2,5-dimethylpiperazine) (TPBM-14) under high pressure. Which exhibited tunable photoluminescence (PL) emission from red to yellow orange. Meanwhile, the band gap continued to decrease below 20.0 GPa, accompanied by piezochromism, which was associated the shrinkage and distortion of inorganic, which enhances the crystal field splitting energy and reduces the energy gap of the $^4T_1$ to $^6A_1$ transition. The unique octahedral corner- and edge-sharing structure of (TDMP)$PbBr_4$, the synergistic effect of Mn doping and pressure induces local lattice distortion in TPBM-14, leading to a significant enhancement of the STE emission at 8.1 GPa. Our research explores the intrinsic connection between the band structure and optical properties of TPBM-14 under high pressure and offers valuable insights for performance optimization.

© 2025 Published by Elsevier B.V. on behalf of Chinese Chemical Society and Institute of Materia Medica, Chinese Academy of Medical Sciences.

1D organic-inorganic lead (Pb) halide perovskites exhibit unique optical properties, such as high luminescence quantum efficiency, large absorption coefficient, and wide tunable range of luminescence colors, demonstrating remarkable performance in photoelectric field [1–6]. The toxicity and instability of Pb have greatly stimulated research in modifying the existing perovskite materials [7–9]. Among the array of modulation approaches, metal ion doping has emerged as an effective approach for tailoring chemical composition and tuning optoelectronic characteristics by exciton-dopant coupling. This strategy affords a variety of opportunities for endowing metal halide perovskites (MHPs) with new optical, electronic and magnetic properties, enabling the development of multifunctional materials [10–15]. To date, a variety of metal ions have been intentionally incorporated into MHPs frameworks [16–18]. Notably, Mn^{2+} exhibit considerable promise owing to their high luminous efficiency and non-toxic characteristics. Within Mn^{2+}-doped perovskite systems, the intense exchange interaction among charge carriers enables Mn^{2+} d electrons to mediate efficient energy transfer pathways. This mechanism overcomes the parity-forbidden nature of the $^4T_1$ to $^6A_1$ electronic transition within the octahedral crystal field, ultimately generating prominent red-light emission with high color purity [19–21]. Furthermore, the integration of intrinsic narrow emission and broad dopant emission enhances opportunities for diversifying the luminescent properties of perovskite. Thus, it is pivotal for exploring the relationship of structure and optical properties for Mn^{2+}-doped perovskite.

Pressure, is an effective device for probing the electronic and structural profiles of MHPs. It enables the compression of crystal lattices, leading to tighter atomic packing and reduced interatomic distances, which effectively alters electron orbitals and bonding configurations [22–27]. In the recent period, high-pressure studies on MHPs have garnered increasing attention. Systematic investigations into the behavior of MHPs under pressure have provided valuable insights into the structure-property relationship [28–36]. Several novel properties have been identified, such as enhanced structural stability, pressure-induced emission (PIE), pressure-induced emission enhancement (PIEE), and metallization effects [37–44]. In addition, Cao *et al.* reported pressure-induced emission enchantment for Mn^{2+}-doped $CsPbCl_3$ (3D) nanocrystals (NCs) at a specific pressure threshold of 1.41 GPa [45].

* Corresponding authors.
E-mail addresses: wangguangxia1107@126.com (G. Wang), zengqg1979@126.com (Q. Zeng), xguanjun@jlu.edu.cn (G. Xiao).

https://doi.org/10.1016/j.cclet.2025.111507
1001-8417/© 2025 Published by Elsevier B.V. on behalf of Chinese Chemical Society and Institute of Materia Medica, Chinese Academy of Medical Sciences.

Shi *et al.* demonstrated the manipulation of optical properties within Mn^{2+}-doped 2D $(PEA)_2PbBr_4$ ($PEA^+ = C_6H_5C_2H_4NH_3^+$) NCs, achieving a continuous narrowing of the bandgap and significant piezochromism [46]. Zhang *et al.* realized an extensive reduction in the bandgap by up to 12.2 % through compression-decompression cycles in Mn-doped $Cs_2NaBiCl_6$, with the Mn^{2+} emission being markedly augmented under pressure [47]. These findings indicate that the synergistic effect of Mn^{2+} doping and pressure can effectively modulate the optical properties. It is necessity for further research into the structural and optical properties of Mn^{2+}-doped 1D MHPs under high pressure.

Here, we systematically investigated the structural evolution and optical properties of TPBM-14 under high pressure. This finding reveals that the compound exhibits reversible pressure-induced emission tuning, transitioning from red to yellow-orange emissions accompanied by pressure-induced emission quenching. A series of *in situ* high-pressure experiments were regulated to examine the structural evolution and luminescence mechanism associated with Mn^{2+} doping under high pressure. This work offers valuable insights into the relationship between emission behavior and structure in 1D perovskites following Mn doping, and provides a new thought for designing new perovskites with excellent optoelectronic properties.

The $(TDMP)PbBr_4$ and Mn-doped $(TDMP)PbBr_4$ with varying doping ratios were prepared by cooling-crystallization. The XRD diffraction peaks of all samples were in agreement with the previously reports (Fig. 1a), confirming that Mn^{2+}-doped $(TDMP)PbBr_4$ was successfully prepared without any impurity phase [48–50]. As the concentration of Mn^{2+} increased, the diffraction peaks shifted systematically toward lower angles, which could be attributed to the stronger complexation affinity of Mn^{2+} with diamine ligands compared to Pb^{2+}. The Mn^{2+} preferentially interact with amine groups in organic molecules, subsequently occupying interstitial sites within the organic layers. This substitution-induced lattice expansion ultimately leads to a slight enlargement of the crystal lattice. The morphological characterization of the synthesized samples was shown in Fig. 1b and Fig. S1 (Supporting information). TDMP-14 (the Pb:Mn ratio is 1:14) exhibits rod-like structures with length exceeding several hundred micrometers and diameters of approximately 10 μm. Elemental mapping reveals homogeneous distribution of Pb, Br, and Mn elements throughout the Mn^{2+}-doped $(TDMP)PbBr_4$. PL performance testing of both pristine and doped samples (Fig. 1c) demonstrates that $(TDMP)PbBr_4$ displayed broad white emission, including the FE state (at 380 nm) and STE state (at 510 nm), respectively. Previous research demonstrated the STE emission was fundamentally related to Jahn-Teller distortion within the octahedral lattice [49,50]. After doping with Mn^{2+}, three PL peaks emerge: FE, STE and an additional broad peak at 640 nm attributed to the ligand-field transition ($^4T_1$ to $^6A_1$) of Mn^{2+}, consistent with previous reports [49]. Notably, when the Pb:Mn ratio reaches 1:14, the emission intensity maximizes at 640 nm with a photoluminescence quantum yield (PLQY) of 92 % (Fig. 1d).

To demonstrate that Mn-doped $(TDMP)PbBr_4$ possesses multiple emission centers and to explore the luminescence mechanism after Mn^{2+}-doped, we performed time-resolved photoluminescence measurements on it. Fig. 1e and Fig. S2 (Supporting information) display the PL decay lifetime curves at 380, 510, and 640 nm. For the emissions from free excitons FE and STE, their lifetimes are only on the nanosecond scale and gradually decrease upon increasing Mn^{2+} doping ratio. Which is due to Mn^{2+}-doped provides additional energy transfer pathways for FEs. After Mn^{2+}-doped, the lifetime extends to the millisecond scale and remains unchanged with varying doping concentrations, which is consistent with reports on Mn-doped perovskites and other materials [51–53].

To check into the optical properties of Mn-doped $(TDMP)PbBr_4$, we implemented *in situ* high-pressure PL measurements on TPBM-14 (Figs. 2a and b). With pressure increases, all three PL peaks exhibit noticeable red shifts, accompanied by a broadening of full width at half-maximum (FWHM). Specifically, Mn^{2+}-related emission peak red-shifts significantly from 640 nm to 710 nm as the pressure reaches 6.4 GPa. Upon pressure reaches to 20.5 GPa, the PL peak continues to red-shift to 735 nm (Fig. 2c). Moreover, the PL intensities of all three peaks gradually decrease and vanish completely at 6.4 GPa (Fig. 2d). Surprisingly, the STE emission intensity exhibits a sudden increase at 8.1 GPa, followed by a decrease and eventual quenching at 20.5 GPa. In addition, due to its unique post-perovskite chains composed of octahedra with shared corners and edges and the inherent spatial effects that limit the distortion of the octahedra, Mn-doped $(TDMP)PbBr_4$ exhibited significant differences in optical properties compared to Mn-doped 2D perovskite $(PEA)_2PbBr_4$ nanocrystals (NCs) (4.4 GPa) [46] and Mn-doped 3D perovskite $CsPbBr_3$ NCs (5.8 GPa) [43]. As pressure is increased, the color transitions of PL from bright red to dark red which can be clearly observed in PL micrographs and intensity of PL peaks (Fig. 2e). Above 6.4 GPa, the PL color shifts to yellow and eventually faded away at 20.5 GPa, aligning with the color transition observed in $(TDMP)PbBr_4$ between 4.0 GPa and 20.0 GPa (Fig. S4 in Supporting information) [48]. Meanwhile, *in situ* high-pressure PL measurements of samples with varying ratios show red-shifting of all

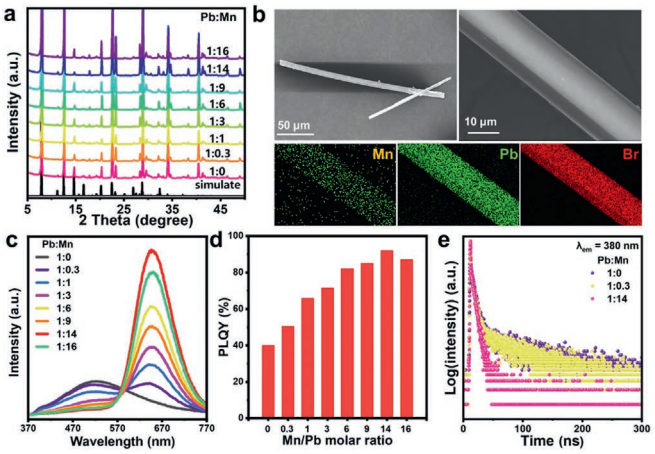


Fig. 1. (a) The XRD pattern and simulated diffraction pattern of $(TDMP)PbBr_4$ with different Mn doping ratios. (b) SEM images and corresponding element mappings of Pb, Br in TDMP-14 microrods. (c) The PL spectra and (d) PLQY of $(TDMP)PbBr_4$ with different Mn^{2+} doping ratios. (e) PL decay lifetime curves at 640 nm.

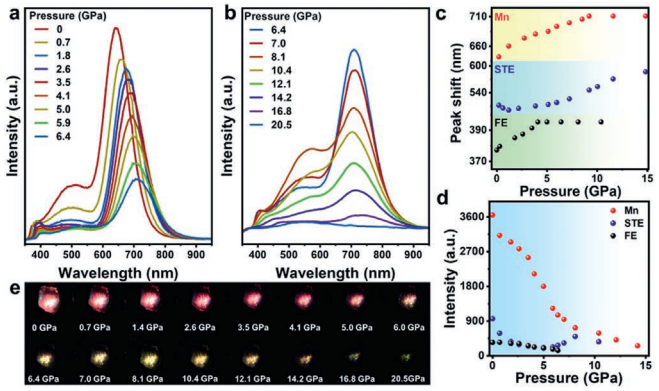


Fig. 2. (a, b) The pressure-dependent PL spectra of TPBM-14 microrods from 0 to 20.5 GPa. (c) The PL peaks shift of TPBM-14 microrods from 0 to 14.2 GPa. (d) Pressure-induced evolution of PL micrographs. (e) The intensity of all PL peaks under compression.

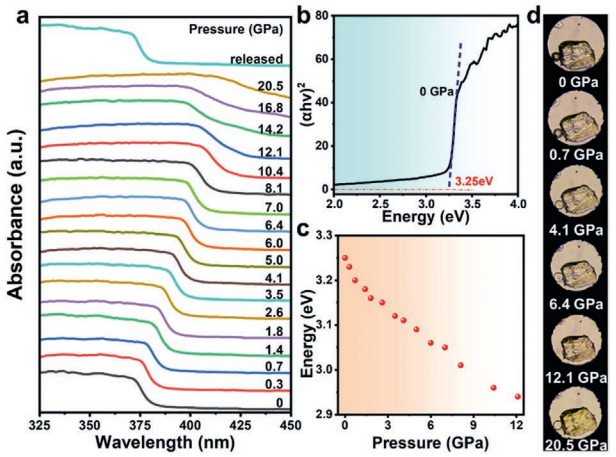


Fig. 3. (a) The UV–vis absorption spectra of TPBM-14 at various pressures. (b) The bandgap Tauc plots for TPBM-14 at ambient conditions (0 GPa). (c) Bandgap evolution of TPBM-14 at various pressures. (d) The optical micrographs of TPBM-14 under different pressures.

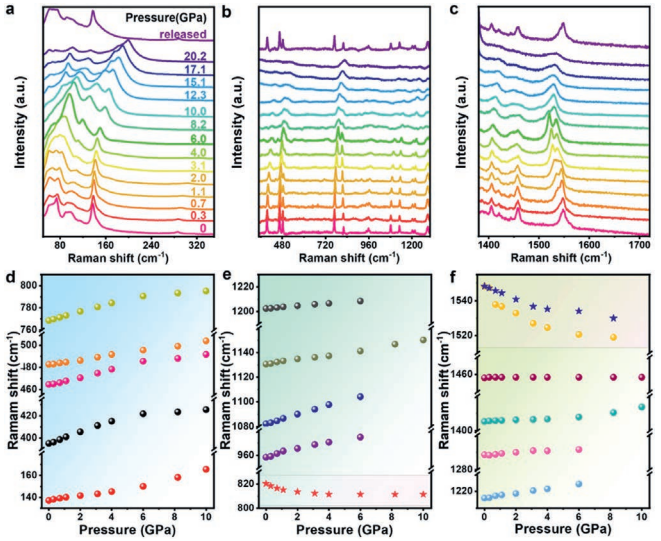


Fig. 4. (a-c) Typical Raman spectra of TPBM-14 microrods from 0 to 20.2 GPa. (d-f) The Raman shift of TPBM-14 microrods under high pressure.

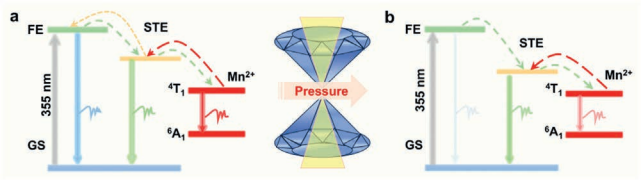


Fig. 5. Schematic illustrations of emission evolution by configuration coordinate diagram upon compression. The term GS, FE and STE in the diagram represent Ground state, free exciton state, and self-trapped exciton state, respectively.

PL peaks under pressure, as further evidenced by the fluorescence images (Fig. S5 in Supporting information). Compared to the color change of (TDMP)$PbBr_4$, the lattice expansion caused by Mn^{2+} doping for initial structure requires higher pressure. These results demonstrate that both TPBM-14 and (TDMP)$PbBr_4$ exhibit significantly pressure-tunable emission behaviors. In addition, following decompression, the PL spectra recovered their original shape and position; however, the intensity remained slightly lower than that at ambient pressure (Fig. S6 in Supporting information).

In addition, the modulation of the band gap can visually reflect the variations in optical properties of metal halide perovskites under high pressure. To further investigate the evolution of TPBM-14 optical properties, we performed *in situ* high-pressure absorption spectrum experiments ranging from ambient conditions to 20.5 GPa. The absorption spectra are illustrated in Fig. 3a with pressure as the independent variable, revealing a significant regularity in their evolution with increasing pressure. In usual atmospheric pressure, the absorption edge of TPBM-14 is located at 375 nm, and no significant change is observed after doping, which is in accordance with previous findings [49]. The bandgap value is determined to be 3.25 eV (Fig. 3b) calculated by extrapolating the linear region of $(\alpha h\upsilon)^2$ *versus* $h\upsilon$ in Tauc plots, where α is the absorption coefficient and $h\upsilon$ is the photon energy. As the pressure increases, the absorption edge exhibits a continuous redshift, consistent in the redshift observed in all three PL peaks. In addition, this trend is similar with the absorption edge evolution observed in (TDMP)$PbBr_4$ (Fig. S7 in Supporting information) [48]. When the pressure reaches 20.5 GPa, the bandgap value of TPBM-14 decreases from 3.25 eV to 2.76 eV (Fig. 3c). A sharp decline in the bandgap was observed above 12.1 GPa, which was consistent with the pressure point at which PL begin to quench. It is attributed to lattice contraction under high pressure and potential structural amorphization induced by extreme compression. Upon completely release of pressure, the absorption spectra of pressure-treated TDMP-14 displayed a subtle deviation from its original state. Furthermore, optical micrographs recorded under high pressure (Fig. 3d) demonstrate a distinct color evolution of TDMP-14, transitioning from colorless to yellow. This observation highlights a remarkable piezochromic effect under compression.

To further investigate the structural origin of optical properties changes, the *in situ* high-pressure Raman spectroscopy experiments on TPBM-14 was conducted (Figs. 4a-c). The low-frequency lattice vibrational modes (50–350 cm^{-1}) correspond to Pb-Br and Mn-Br vibrational modes within the inorganic framework, characterized by ionic and covalent interactions. In contrast, the intramolecular vibrational modes of the organic constituents appeared in the higher frequency region (above 350 cm^{-1}) [49,50]. With increasing pressure, the low-frequency lattice vibrational modes exhibit a normal blue-shift, reflecting progressive inorganic lattice contraction. Meanwhile, most vibrational modes of the organic moieties exhibit slightly blue shift to higher wavenumbers and unobvious adjusted intensity (Figs. 4d-f), which indicates that the degree of inorganic lattice distortion under pressure is greater than that of the organic cations. Additionally, the CH_2/NH_2 cyclic rocking mode at 820 cm^{-1} and the NH_2 rocking mode at 1549 cm^{-1} display anomalous red shift, which is attributed to the combination of motional constraints and deformation of the organic cations coupled with lattice compression. At approximately 8.2 GPa, vibrational modes exhibit obvious variations, indicating obvious local tilting and distortions in the inorganic sublattices. This observation provides further insight into the enhanced STE emission detected at this pressure threshold, which is ascribed to the strengthened phonon-electron coupling induced by pressure-driven lattice distortions. When the pressure reaches 12.3 GPa, the disappearance of specific Raman peaks combined with broadening and weakening of other vibrational modes suggest the partial disordering within both the inorganic and organic components. The Raman experiments support the proposed PL emission quenching and absorption edge broadening that TPBM-14 begins to amorphized after 12.0 GPa. When the pressure is fully released, the amorphous characteristics reflected in the Raman signals revert to their original state, aligning with the changes detected in the PL and absorption spectra.

Based on the above experimental analysis, the photophysical process of TPBM-14 is shown in Fig. 5. Under environmental conditions, the $^4T_1$ to $^6A_1$ transition of Mn^{2+} creates a new emis-

sion channel at 640 nm in (TDMP)$PbBr_4$, resulting in red emission for TPBM-14. Under UV excitation, the TPBM-14 is initially excited to the FE state, followed by relaxation to the STE state and the d-d transition of Mn, the latter of which can return to the FE state *via* radiative recombination (Fig. 5a). After compression, the intensity of all PL peaks decreases, accompanied by a significant redshift in PL peak positions, due to lattice contraction caused by pressure, which increases the crystal field splitting energy and reduces the energy gap of $^4T_1$ to $^6A_1$ transition. Strong electron-phonon interactions also hinder d-d transition relaxation from FE to Mn pair configurations. The redshift observed in absorption spectra further supports this result. Compared with Mn-doped 2D $(PEA)_2PbBr_4$ NCs and Mn-doped 3D $CsPbBr_3$ NCs, the pressure point of PL emission tuning was hysteretic, resulting from the unique post-perovskite chains composed of octahedra with shared corners and edges and the inherent spatial effects [43,46]. Meanwhile, the struggle between interlayer contraction and lattice distortion drives moderate band-gap narrowing. Above 8.1 GPa, the abnormal enhancement of the STE emission can be attributed to the distortion and deformation of the inorganic lattice, which prevents the excitons in the STE state from being recaptured return to the state of FE (Fig. 5b), suggesting that enhanced phonon coupling obstructs the transition of excitons from the STE state back to their respective FE states.

In summary, we systematically investigated the connection between the optical properties and structural evolution of Mn-doped 1D post-perovskite (TDMP)$PbBr_4$ under high pressure. We successfully achieved the pressure-tunable emission from red to yellow, attributed to the compression of Mn-Br bond caused by octahedral contraction, which intensifies crystal field splitting and facilitates the $^4T_1$ to $^6A_1$ transition. In addition, due to its unique post-perovskite chains composed of octahedra with shared corners and edges and the inherent spatial effects, Mn^{2+}-doped (TDMP)$PbBr_4$ exhibited significant differences in optical properties compared to Mn-doped 2D $(PEA)_2PbBr_4$ NCs and 3D $CsPbBr_3$ NCs. Simultaneously, the bandgap progressively diminished from an initial 3.25 eV to 2.76 eV, accompanied by a pronounced piezochromic effect. The Raman spectroscopy under high pressure further indicated that the optical properties changes are closely connected with the contraction and distortion of octahedra. Our study reveals the relationship between the structure and optical properties of Mn-doped 1D post-perovskites under high pressure, providing critical insights into the physical and chemical mechanisms of Mn-doped organic-inorganic MHPs systems under high pressure and further broadening their applications in optoelectronic.

Declaration of competing interest

The authors declare that they have no known competing financial interests or personal relationships that could have appeared to influence the work reported in this paper.

CRediT authorship contribution statement

Ruijing Fu: Writing – original draft, Visualization, Funding acquisition, Conceptualization. **Junpeng Gao:** Validation, Methodology, Data curation. **Lingrui Wang:** Supervision, Funding acquisition. **Bin Xiao:** Methodology, Data curation. **Guangxia Wang:** Supervision, Funding acquisition. **Qingguang Zeng:** Supervision, Funding acquisition. **Guanjun Xiao:** Writing – review & editing, Visualization, Supervision, Funding acquisition.

Acknowledgments

This work was supported by the National Natural Science Foundation of China (Nos. 12404024, 12474414, 12174144, 12474009), the Natural Science Foundation of Guangdong Province (Nos. 2023A1515012706, 2022A1515011669), the Cooperative education platform of Guangdong Province (No. (2016)31), the Open Project of State Key Laboratory of Superhard Materials, Jilin University (No. 202414), the Guangdong Basic and Applied Basic Research Foundation (No. 2020A1515110120), the Major Science and Technology Research and Development Project of Jiangxi Province (No. 20223AAE01003), Basic and Applied Basic Research Foundation of Jiangmen (No. 2020030102940008548), the Science Foundation for High-level Talents of Wuyi University (Nos. 2021AL019, 2019AL029).

Supplementary materials

Supplementary material associated with this article can be found, in the online version, at doi:10.1016/j.cclet.2025.111507.

References

[1] X. Xu, X. Zhang, W. Deng, J. Jie, X. Zhang, Small Methods 2 (2018) 1700340.
[2] W. Zhang, K. Tao, C. Ji, et al., Inorg. Chem. 57 (2018) 4239–4243.
[3] Q. Zhou, W. Li, J. Xiao, A. Li, X. Han, Adv. Funct. Mater. 34 (2024) 2402902.
[4] C. Zhou, Y. Tian, M. Wang, et al., Angew. Chem. Int. Ed. 56 (2017) 9018–9022.
[5] G. Huang, H. Zhou, C. Wang, et al., Inorg. Chem. Commun. 128 (2021) 108581.
[6] Y. Peng, Y. Yao, L. Li, et al., J. Mater. Chem. C 6 (2018) 6033–6037.
[7] X. Ding, R. He, T. Zhang, et al., ACS Appl. Mater. Interfaces 15 (2023) 42139–42152.
[8] A. Jha, P. Bansal, G.K. Nim, P. Kar, Opt. Mater. 111 (2021) 110660.
[9] L. Mei, R. Xie, S. Zhu, et al., Nano Today 50 (2023) 101830.
[10] A. Chu, J. Luo, Z. Xu, et al., J. Mater. Chem. C 12 (2024) 9733–9741.
[11] H. Li, K. Han, Z. Li, et al., Adv. Sci. 11 (2024) 2307354.
[12] S. Mukherjee, S. Ghosh, D. Biswas, et al., Nanoscale 15 (2023) 6947–6953.
[13] X. Wang, Q. Shen, Y. Chen, et al., Nanoscale 13 (2021) 15285–15291.
[14] B. Zhou, Z. Liu, S. Fang, et al., J. Phys. Chem. Lett. 13 (2022) 9140–9147.
[15] S. Ge, Q. Wei, W. Jia, et al., Appl. Phys. Lett. 118 (2021) 152102.
[16] S. Wang, J. Leng, Q. Sun, C. Zhao, S. Jin, J. Phys. Chem. Lett. 12 (2021) 1475–1480.
[17] A. Karmakar, M.S. Dodd, S. Agnihotri, E. Ravera, V.K. Michaelis, Chem. Mater. 30 (2018) 8280–8290.
[18] W. Li, Y. Wang, H. Yin, et al., Inorg. Chem. 23 (2024) 10481–10489.
[19] B. Su, G. Zhou, J. Huang, et al., Laser Photonics Rev. 15 (2021) 2000334.
[20] J. Gao, Y. Guo, X. Zhang, et al., Adv. Sci. 12 (2025) 2413402.
[21] S. Ji, X. Yuan, S. Cao, et al., J. Phys. Chem. Lett. 11 (2020) 2142–2149.
[22] Z. Ma, Q. Li, J. Luo, et al., J. Am. Chem. Soc. 143 (2021) 15176–15184.
[23] Y. Wang, X. Yang, C. Liu, et al., Angew. Chem. Int. Ed. 61 (2022) e202210836.
[24] T. Zhang, X. Yong, J. Yu, et al., Adv. Mater. 35 (2023) 2211729.
[25] Z. Ma, G. Xiao, L. Ding, J. Semicond. 42 (2021) 100203–100204.
[26] A. Noculak, S.C. Boehme, M. Aebli, et al., Helv. Chim. Acta 104 (2021) e2000222.
[27] A. Weingarten, Nat. Rev. Chem. 3 (2019) 513 -513.
[28] Y. Chen, R. Fu, L. Wang, et al., J. Mater. Chem. A 7 (2019) 6357–6362.
[29] Z. Ma, F. Li, G. Qi, et al., Nanoscale 11 (2019) 820–825.
[30] G. Xiao, Y. Wang, D. Han, et al., J. Am. Chem. Soc. 140 (2018) 13970–13975.
[31] R. Fu, W. Zhao, L. Wang, et al., Angew. Chem. Int. Ed. 60 (2021) 10082–10088.
[32] N. Li, Q. Zhang, Y. Wang, W. Yang, Appl. Phys. Lett. 117 (2020) 080502.
[33] G. Xiao, T. Geng, B. Zou, ACS Mater. Lett. 2 (2020) 1233–1239.
[34] Q. Li, B. Xu, X. Xu, Y. Wang, Z. Quan, Aggregate 6 (2025) e70004.
[35] N.V. Morozova, I.V. Zhevstovskikh, I.V. Korobeinikov, et al., J. Alloy. Compd. 988 (2024) 174305.
[36] D. Zhao, M. Cong, Z. Liu, et al., Cell Rep. Phys. Sci. 4 (2023) 101445.
[37] Z. Ma, Z. Liu, S. Lu, et al., Nat. Commun. 9 (2018) 4506.
[38] Y. Shi, Z. Ma, D. Zhao, et al., J. Am. Chem. Soc. 141 (2019) 6504–6508.
[39] Y. Fang, L. Zhang, L. Wu, et al., Angew. Chem. Int. Ed. 58 (2019) 15249–15253.
[40] W. Zhao, G. Xiao, B. Zou, Aggregate 5 (2024) e461.
[41] Y. Wang, S. Guo, H. Luo, et al., J. Am. Chem. Soc. 142 (2020) 16001–16006.
[42] X. Yu, Y. Fang, X. Sun, et al., Angew. Chem. Int. Ed. 63 (2024) e202412756.
[43] Y. Shi, W. Zhao, Z. Ma, G. Xiao, B. Zou, Chem. Sci. 12 (2021) 14711–14717.
[44] M. Cong, Q. Li, X. Wang, et al., ACS Mater. Lett. 7 (2025) 996–1002.
[45] Y. Cao, G. Qi, L. Sui, et al., ACS Mater. Lett. 2 (2020) 381–388.
[46] Y. Shi, Z. Jin, P. Lv, et al., J. Mater. Chem. C 11 (2023) 1726–1732.
[47] L. Zhang, Z. Liu, X. Sun, et al., Adv. Optical Mater. 10 (2022) 2101892.
[48] R. Fu, J. Gao, L. Wang, et al., Inorg. Chem. 63 (2024) 18276–18284.
[49] R. Gautier, F. Massuyeau, G. Galnon, M. Paris, Adv. Mater. 31 (2019) 1807383.
[50] R. Gautier, M. Paris, F. Massuyeau, J. Am. Chem. Soc. 141 (2019) 12619–12623.
[51] T. Huang, H. Peng, Q. Wei, et al., Nano Energy 93 (2022) 106863.
[52] G. Zhou, X. Jiang, M. Molokeev, et al., Chem. Mater. 31 (2019) 5788–5795.
[53] Z. Wang, Y. Xiao, B. Liu, et al., Adv. Opt. Mater. 12 (2024) 2301796.